Journal for Multiscale Computational Engineering 8(5), 509–522 (2010)

CALIBRATION OF NANOCRYSTAL GRAIN BOUNDARY MODEL BASED ON POLYCRYSTAL PLASTICITY USING MOLECULAR DYNAMICS SIMULATIONS

Sangmin Lee & Veera Sundararaghavan*

Department of Aerospace Engineering, University of Michigan, Ann Arbor, MI 48109, USA

*Address all correspondence to Veera Sundararaghavan E-mail: vs85@cornell.edu

Decohesion parameters are computed for the tilt grain boundaries through molecular simulations and the parameters are employed in a elastoplastic deformation model of a face-centered-cubic nanocrystal. The calibrated continuum grain boundary model accounts for reversible elastic and irreversible inelastic separation sliding deformations. The intragranular plasticity was modeled using a rate-independent single-crystal plasticity model. Atomistic calculations are presented for a planar, copper grain boundary interface with a tilt lattice misorientation for cases of loading and unloading. The interface models are deformed to full separation and then relaxed to study inelastic behavior. Plots of stress versus displacement show a distinctly different deformation response between normal and tangential interface loading conditions. Two-dimensional microstructures uniaxially loaded using the calibrated cohesive model indicate that the macroscopically observed nonlinearity in the mechanical response is mainly due to the inelastic response of the grain boundaries. Plastic deformation in the interior of the grains prior to the initiation of grain boundary cracks was not observed. Although key features of the molecular simulation results have been introduced in the cohesive model, a few discrepancies between the behavior of cohesive model when compared to molecular simulations are noted.

KEY WORDS: *nanocrystals, fracture, crystal plasticity, molecular dynamics, cohesive elements*

1. INTRODUCTION

Metallic nanocrystals are interesting engineering materials due to their high yield strength and high strain hardening rates, leading to very high tensile strengths. Recent experiments [transmission electron microscopy study in Kumar et al. (2003)] as well as molecular simulations (Swygenhoven et al., 1999; Schiøtz et al., 1999; Swygenhoven, 2004; Yamakov et al., 2006, 2001) have indicated that inelastic deformation in nanocrystals primarily originates from grain boundary accommodation effects, such as grain boundary sliding and separation. Grain boundary models have been developed in the past to describe the brittle failure behavior of metallic materials. Grain boundaries have been incorporated as volume elements with simple isotropic-type hardening rules (Fu et al., 2004). These approaches fail to explain the sliding and fracture behavior observed in grain boundaries.

In recent years, cohesive interface models have emerged as attractive methods to numerically simulate fracture initiation and growth by the finite element method (Needleman, 1990, 1992; Tvergaard et al., 1993, 1996; William, 1989; Camocho et al., 1997; Xu and Needleman, 1994; Ortiz and Pandolfi, 1999; Zavattieri and Espinosa, 2001). Typically, a cohesive interface is introduced in a finite element discretization of the problem by the use of special interface elements, which obey a nonlinear interface traction separation constitutive relation. These relations provide a phenomenological description for the complex atomistic processes that lead to the formation of new traction-free crack faces. The grain boundary parameters in these models are either phenomenologically assumed or calibrated from experiments. Thus, these models consider the macroscopic effects without resolving the atomistic scale details. Although potentials for interplanar glide at the contin-

1543–1649/10/$35.00

uum scale can be defined based on atomic level details [e.g., dislocation nucleation (Rice, 1992)], they do not have a strong physical basis for coupling shear and normal tractions and do not account for irreversibilities in the tractionseparation process. These irreversibilities include path history effects associated with nonuniform distribution of bond ruptures and dislocation emission at nanoscales.

Recently, Wei and Anand (2004) have proposed an elasticplastic interface model that accounts for irreversible inelastic separation and sliding deformations at the interface prior to failure. In addition to a traction-separation relation for normal separation across an interface, appropriate relations for combined opening and sliding are also developed in an approach similar to single-crystal dislocation plasticity formulations. In the approach, parameters were obtained by calibration with experimental stress-strain curves, which makes it difficult to unambiguously define the GB properties such as the strengths in the tensile and shear modes. Furthermore, continuum models cannot be directly verified without atomistic calculations because their validity is contingent on the accuracy of parameters used in the phenomenological model. The nanoscopic length scales involved in the model is directly accessible from molecular simulations and will allow one to calibrate the model directly from atomistic simulations, although at high deformation rates. With the advent of parallel processing, large-scale atomistic calculations have been performed to address such effects (Nakano et al., 1994; Holian and Ravelo, 1995; Zhou et al., 1998; Cleri et al., 1997, 1998). Recently, quasicontinuum simulation of the interface (Warner et al., 2006) has been used to identify the normal and shear strengths of the GBs for use in a continuum model. Methods for calibrating such cohesive elements using results from molecular dynamic MD simulations has also been recently studied (Spearot et al., 2004; Gall et al., 2000; Sundararaghavan and Zabaras, 2006). In this approach, tensile and shear tests are performed on a bicrystal interface using molecular dynamics to obtain the cohesive response of the interface. We further investigate the use of this method (Spearot et al., 2004) to calibrate cohesive models and perform continuum finite element simulations of nanocrystals. This continuum model uses rate-independent crystal plasticity theory for the grain interior to model nanoscale intragranular behavior. Interface constitutive model employed in this work allows for inelasticity at the interface prior to failure. To capture the cohesive law obtained from MD simulations, we focus on calibrating the parameters in the equations governing evolution of scalar state variables of the interface. The mechanical response of a nanocrystal with initially random orientation distribution is investigated using this approach, and the physical origin of macroscopically observed nonlinearity in the stress-strain response is investigated. In addition, these simulations are used to obtain information on the effect of stress concentrations at the tips of grain boundary cracks and at triple junctions on overall plastic deformation. The applicability of the cohesive model is studied and discrepancies occurring between the continuum model and the molecular simulations are identified, especially, in the unloading and reloading behavior for the normal separation mode.

The paper is organized as follows. In Section 2, the continuum grain boundary model is described. An elastic potential is introduced for interface separation, which admits a dependence of a cohesive interface potential on a set of state variables (for the isothermal case) that characterize the interface structure and morphology. To account for separation associated with irreversible processes, defined as plastic separation, the rate of change of the constituents that characterize the internal structure within the interface region are tracked by a set of state variables over the course of the deformation. In Section 3, MD simulation results are presented for normal and tangential separation of a copper bicrystal with a planar interface structure. The continuum formulation that uses the molecular simulation results is based on calibration of state variable evolution equations for the interface. In Section 4, simulation results for crack initiation processes in a nanocrystal are presented.

2. COHESIVE ELEMENT TECHNIQUE FOR SIMULATING MECHANICAL RESPONSE IN NANOCRYSTALLINE MATERIALS

Let $\boldsymbol{x} : \mathcal{B}_n \rightarrow \mathcal{B}$ represent the nonlinear deformation map of the nanocrystal at time t, and $\boldsymbol{F} = \nabla_n \boldsymbol{x}$ the associated tangent map. $\boldsymbol{F}$ maps points $\boldsymbol{X} \in \mathcal{B}_n$ onto points $\boldsymbol{x}(\boldsymbol{X}, t)$ of the current configuration $\mathcal{B}_{n+1}$.

The kinematic problem for deformation employs the updated Lagrangian framework. Here, the total deformation gradient $\boldsymbol{F}_{n+1}$ at time $t = t_{n+1}$ of configuration $\mathcal{B}_{n+1}$ with respect to the initial undeformed configuration $\mathcal{B}_0$ (with points $\boldsymbol{X}_0$) at time $t = 0$ is assumed to be decomposed as

$$\begin{aligned} \boldsymbol{F}_{n+1} &= \nabla_0 \tilde{\boldsymbol{x}}(\boldsymbol{X}_0, t_{n+1}) \\ &= \nabla_n \hat{\boldsymbol{x}}(\boldsymbol{X}_n, t) \nabla_0 \tilde{\boldsymbol{x}}(\boldsymbol{X}_0, t_n) \\ &= \boldsymbol{F}_r \boldsymbol{F}_n = \boldsymbol{F}^e \boldsymbol{F}^p \end{aligned} \tag{1}$$

where $\boldsymbol{F}^e$ and $\boldsymbol{F}^p$ are the elastic and plastic deformation gradients respectively at time $n+1$, $\boldsymbol{F}_r$ is the relative deformation gradient of the current configuration with respect to the configuration at time n, and $\boldsymbol{F}_n$ refers to the total deformation gradient in the reference configuration ($\mathcal{B}_n$) with respect to the initial undeformed configuration.

The equilibrium equation is expressed in the reference configuration $\mathcal{B}_n$ as

$$\nabla_n \cdot \boldsymbol{P}_r = \boldsymbol{0} \tag{2}$$

where the PK-I stress $\boldsymbol{P}_r(\boldsymbol{X}_n, t)$ is expressed in terms of the Cauchy stress ($\boldsymbol{T}$) as $\boldsymbol{P}_r(\boldsymbol{X}_n, t) = (\det \boldsymbol{F}_r)\boldsymbol{T}\boldsymbol{F}_r^{-T}$.

A crack at time step n in a cohesive formulation is represented as a surface $\delta\mathcal{B}_n^{int}$ (refer Fig. 1). Tractions $\boldsymbol{t}_n$ at the interface perform work on the displacement jump $[|\boldsymbol{u}|]$ across the cohesive interface. The solution of a generic loading increment involves the solution to the principle of virtual work (PVW) given as follows: Calculate $\boldsymbol{x}(\boldsymbol{X}_n, t)$ such that

$$\int_{\mathcal{B}_n} \boldsymbol{P}_r \cdot \nabla_n \tilde{\boldsymbol{u}} dV_n + \int_{\delta\mathcal{B}_n^{int}} \boldsymbol{t}_n \cdot [|\tilde{\boldsymbol{u}}|] dA = 0 \tag{3}$$

for every admissible test function $\tilde{\boldsymbol{u}}$ expressed over the reference configuration $\mathcal{B}_n$. The weak form is solved in an incremental iterative manner as a result of material nonlinearities. The finite element (FE) technique is used for the solution of the weak form. Bilinear quadrilateral elements are used for modeling grain interiors, and four-noded 2D linear elements with initial zero thickness are used to model the cohesive interface. FE procedure has been implemented in an object-oriented and parallel environment in C++ and PetSc parallel toolbox building from our earlier work (Sundararaghavan and Zabaras, 2006b).

2.1 Constitutive Equations for the Grain Boundaries

The model presented here pertains to a two-dimensional analysis. We consider two grains separated by an interface with the local coordinate defined using a normal $\boldsymbol{n}$ and tangent $\boldsymbol{\tau}$ to the interface defining the x- and y-axis, respectively. A rotation matrix $\boldsymbol{R}$ transforms the sample coordinate system to the interface local coordinates. Let δ denotes the displacement jump across the cohesive surface at current time with respect to the undeformed configuration (as shown in Fig. 1). We assume that the displacement jump may be additively decomposed as

$$\boldsymbol{\delta} = \boldsymbol{\delta}^e + \boldsymbol{\delta}^p \tag{4}$$

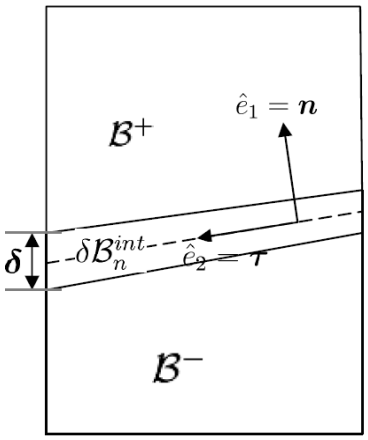

FIG. 1: Cohesive element between two crystals ($\mathcal{B}^+$ and $\mathcal{B}^-$) is shown. The middle surface is taken as the cohesive surface ($\delta\mathcal{B}_n$). The coordinate system for the cohesive element is also shown.

where $\boldsymbol{\delta}^e$ and $\boldsymbol{\delta}^p$ respectively, denote the elastic and plastic parts of the displacement jump. A simple quadratic free energy of the interface is assumed as $\phi = 1/2\boldsymbol{\delta}^e.\boldsymbol{K}\boldsymbol{\delta}^e$ with $\boldsymbol{K}$, the interface elastic stiffness tensor, taken to be positive definite. The traction $\boldsymbol{t}$ is then given by

$$\boldsymbol{t} = \frac{\partial \phi}{\partial \boldsymbol{\delta}^e} = \boldsymbol{K}\delta^e \tag{5}$$

The interface model is taken to be isotropic in its tangential response with interface stiffness tensor taken as $\boldsymbol{K} = K_N \boldsymbol{n} \otimes \boldsymbol{n} + K_T \boldsymbol{\tau} \otimes \boldsymbol{\tau}$ with $K_N > 0$ and $K_T > 0$ the normal and tangential elastic stiffness moduli, respectively. The interface traction $\boldsymbol{t}$ is decomposed into normal and tangential parts, $\boldsymbol{t}_N$ and $\boldsymbol{t}_T$, respectively, over the interface. Scalar state variables $s^{(1)}$ and $s^{(2)}$ are used to represent the deformation resistance for the normal separation and the shear sliding mechanism.

The flow rule for the interface is written as

$$\dot{\boldsymbol{\delta}}^p = \dot{\gamma}^{(1)}\boldsymbol{n} + \dot{\gamma}^{(2)}\boldsymbol{\tau} \tag{6}$$

where $\dot{\gamma}$ is the inelastic deformation rate with the relative plastic displacements defined as $\gamma^{(i)} = \int_0^t \dot{\gamma}^{(i)} dt$. Traction $\boldsymbol{t}$ attains a value of $s^{(i)}$ on the systems where plastic displacements occur. Thus, for $\dot{\gamma} > 0$ the following relationship holds:

$$|\boldsymbol{t}_N| - s^{(1)} = 0 \tag{7}$$

$$|\boldsymbol{t}_T| - s^{(2)} = 0 \tag{8}$$

Interface hardening is defined using an evolution equation for the scalar state variables (from initial value $s^{(i)}(0) = s_0^{(i)}$) as

$$\dot{s}^{(i)} = \sum_{j=1}^{2} \boldsymbol{h}^{(ij)} \dot{\gamma}^{(i)} \tag{9}$$

To capture the cohesive law obtained from MD simulations, we focus on obtaining the right parameters in the above-hardening law. In this work, the evolution of scalar state variables is defined using an equivalent relative plastic displacement defined as

$$\bar{\gamma} = \sqrt{{\gamma^{(1)}}^2 + \alpha {\gamma^{(2)}}^2} \tag{10}$$

with α as the coupling constant, as follows:

$$\dot{s}^{(i)} = h_0^{(i)} \{1 - \frac{s^{(i)}}{s^{*(i)}}\}^{a^{(i)}} \dot{\bar{\gamma}} \quad \text{for} \quad \bar{\gamma} \leq \bar{\gamma}_c \tag{11}$$

$$\dot{s}^{(i)} = -h_{\text{soft}}^{(i)} \dot{\bar{\gamma}} \quad \text{for} \quad \bar{\gamma}_c < \bar{\gamma} \leq \bar{\gamma}_{\text{fail}} \tag{12}$$

$$s^{(i)} = 0 \quad \text{for} \quad \bar{\gamma} > \bar{\gamma}_{\text{fail}} \tag{13}$$

Here, h_0 and h_{soft} are hardening and softening coefficients, respectively; and s^* is the threshold for the interfacial resistance. Here, $\bar{\gamma}_c$ and $\bar{\gamma}_{\text{fail}}$ denote the critical effective displacement and the effective displacement for interface failure. The state variable evolution is calibrated so that the cohesive law as obtained from molecular simulations can be realized.

3. MOLECULAR DYNAMICS FOR GENERATING TRACTION SEPARATION PROFILES FOR GRAIN BOUNDARIES

The MD simulations were designed to mimic simple shear and simple tension for different crystal orientations at different temperatures. The computational setup is illustrated in Fig. 2. The atoms are packed in the domain such that a grain boundary occurs in the middle of the domain. The misorientation between the atoms in the top part of the bicrystal and the bottom part was varied from 15 to 45 deg. There is no rotation about the x- or y-axes, meaning the grain boundary does not have twist characteristics. The width and height of the model after thermal equilibration was 10.84 and 8.31 nm, respectively. This corresponds to about 16 planes of base lattice and 24 planes of the rotated lattice (top) in the y-direction, and the resulting grain boundary was semicoherent. In previous work (Horstemeyer et al., 2001), it was shown that in

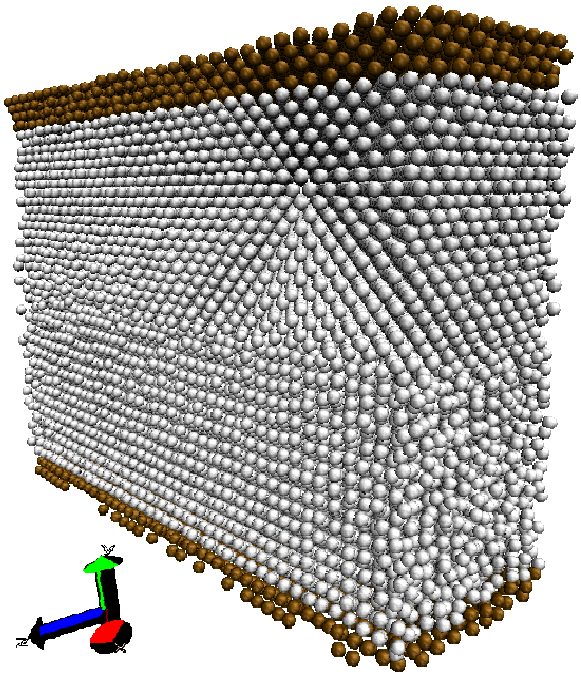

FIG. 2: Initial configuration after equilibration: To deform the grain boundary model with 28000 atoms, uniform displacement rate boundary conditions are applied to the atoms at the top and bottom of the cell.

fixed end simulations, the global continuum stress saturates if the z-direction is four or more unit cells in thickness. The thickness in our simulations is 3.615 nm, corresponding to 20 atomic planes. After creating the samples with a desired crystal orientation, atoms within a thickness along the y-direction of 3.615 A at the bottom and 5.425 A at the top were frozen by assigning zero forces on these atoms.

The embedded atom method (Daw et al., 1993) is used to model the interaction potential between copper atoms in the lattice. Velocities of the interior (or mobile atoms) are initialized using the Maxwell-Boltzmann distribution at room temperature (300 K). These atoms are allowed to relax to minimum energy to accommodate any surface relaxation at the two remaining free surfaces (yz-planes) as well as the grain boundary through equilibration procedure. If just the top row of atoms initially experienced the prescribed velocity without the active internal atoms experiencing the same velocity field, then a shock would be induced into the block of material because of the high strain rates. In our calculations, we introduced an initial

velocity field that mitigated the shock wave and then applied the boundary velocity fields. To accomplish this, the interior atoms in the model were also given an initial x-velocity (superposed on their thermal velocities) that varied linearly from zero to the prescribed velocity at the top atomic plane, depending on their y-coordinates in the simulation box.

To apply tension to the the grain boundary model, uniform displacement rate boundary condition is applied to the top and bottom layer atoms, along the positive and negative y-direction, respectively, as shown in Fig. 2. For both tension and simple shear, the top and bottom layer atoms in Fig. 2 are constrained so that the net force on each atom is set to zero at each time step during the simulation, creating a planar surface. Under application of a prescribed velocity condition, each rigid boundary will move as a single planar and parallel unit during the entire deformation process. For tension simulation, the system is placed in a periodic box along the x and z directions. In the case of simple shear, the computational block of material has free surface in the x direction and was periodic in the z direction. For simple shear, a deformation rate was applied to the block of atoms by setting the x velocity of the top xz plane to a constant value. The bottom atomic plane had a prescribed x velocity of zero for the duration of the simulation. The displacement of the interface region is defined as the sum of the displacements of the loading planes (far-field displacement).

Following initialization, a constant number of atoms, constant volume, and constant temperature (NVT) simulation was performed with a 0.001 ps time step until the block of atoms had undergone complete fracture. Because straining via moving the frozen planes adds considerable energy to the active atoms, a Nose-Hoover thermostat [implemented in LAMMPS software (Plimpton, 1995)] was used during the MD simulation to keep the active atoms at constant temperature. The thermostat applies a damping (or acceleration) factor to the active atoms based on the difference between their current temperature and the desired temperature. To compute the instantaneous temperature of the ensemble of active atoms, one needs to subtract from each atom the nonthermal x velocity that was initially prescribed, since the active atoms essentially maintain the same component of x velocity for the simulation. To qualitatively use the results of the MD simulation to calibrate the nanocrystal continuum model, the average atomic stress (for free atoms) is calculated against boundary displacement in both normal (tensile loading) and tangential (shear loading) directions and the results are discussed in Section 3.1. At each atom, the dipole force tensor, β (known as the local stress tensor), is given by

$$\beta^i_{km} = \frac{1}{\Omega^i} \sum_{j(\neq i)}^{N} f^{ij}_k r^{ij}_m \tag{14}$$

where i refers to the atom in question and j refers to the neighbor atom, f_k is the force vector between atoms, r_m is a displacement vector between atoms i and j, N is the number of neighbor atoms, and Ω^i is the atomic volume. If stress could be defined at an atom, then β would be the stress tensor at that point. Since stress is defined at a continuum point, we determine the stress tensor (termed as the global continuum stress hereafter) as a volume average over the block of material,

$$\sigma_{km} = \frac{1}{N^*} \sum_{i}^{N^*} \beta^i_{mk} \tag{15}$$

in which the stress tensor is defined in terms of the total number of active atoms, N^*, in the block of material.

3.1 MD Results

The grain boundary interface model is loaded to full separation in order to study the quantities that are important for development of a continuum cohesive model for the nanocrystal interface. The quantities include the peak stress, the critical displacement (at peak stress), and the failure displacement (when stress goes to zero). Figure 3 shows the normal stress-displacement response of the grain boundary interface model along with the snapshots of the grain boundary at different times (for a 45 deg misorientation case). Peak stress for tensile failure mode was noted to be about 14 GPa, which is the same as that reported recently (Spearot et al., 2004). Failure displacements cannot be directly compared as this work employs a comparatively larger system size to overcome domain size effect on failure displacements. Although the location of crack depends on the misorientation of the grain boundary, it is generally seen that cracks form at the grain boundaries for misorientations of > 15 deg and the cracks begins with void formation.

We have investigated the stress displacement response of the bicrystal for various values of the misorientations at a temperature of 300 K at an imposed deformation rate of 1 Å/ps and 3 fs time steps. We focus our attention on the three parameters that are used for calibration of the cohesive zone model, namely, the peak stress, σ_p, the critical displacement, δ_{critical}, and the area under the traction separation law (fracture energy). Figure 4 plots the normal

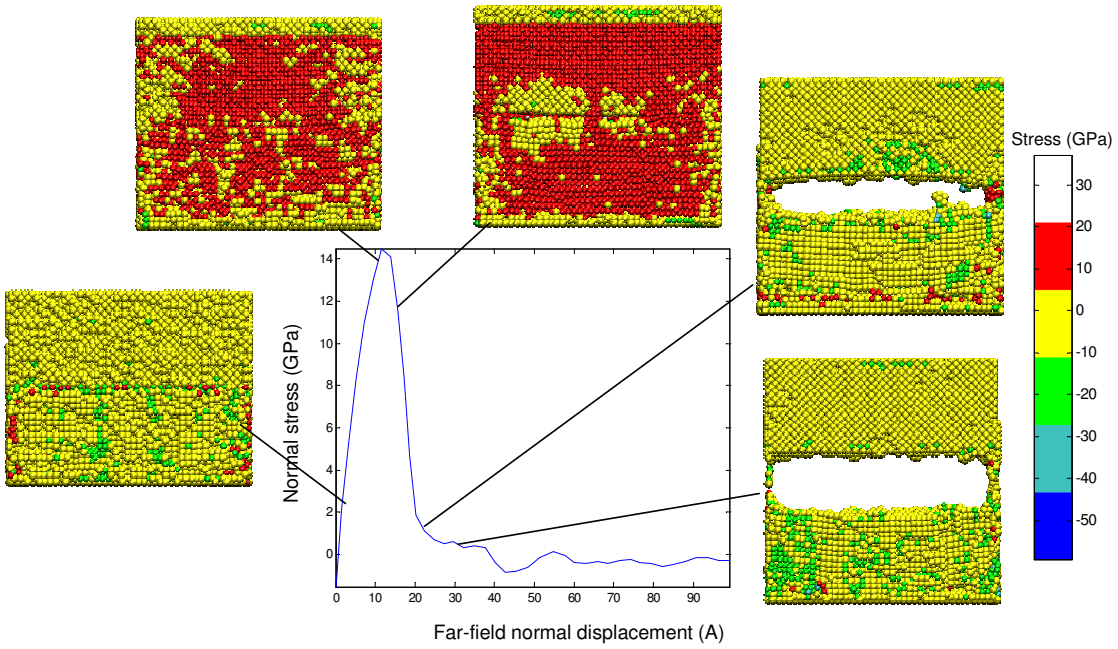

FIG. 3: Normal stress displacement response of the interface model: During tensile separation, the normal stress displacement response shows a dominant peak with associated peak stress. Peak stress is around 14 GPa as reported in (Spearot et al., 2004).

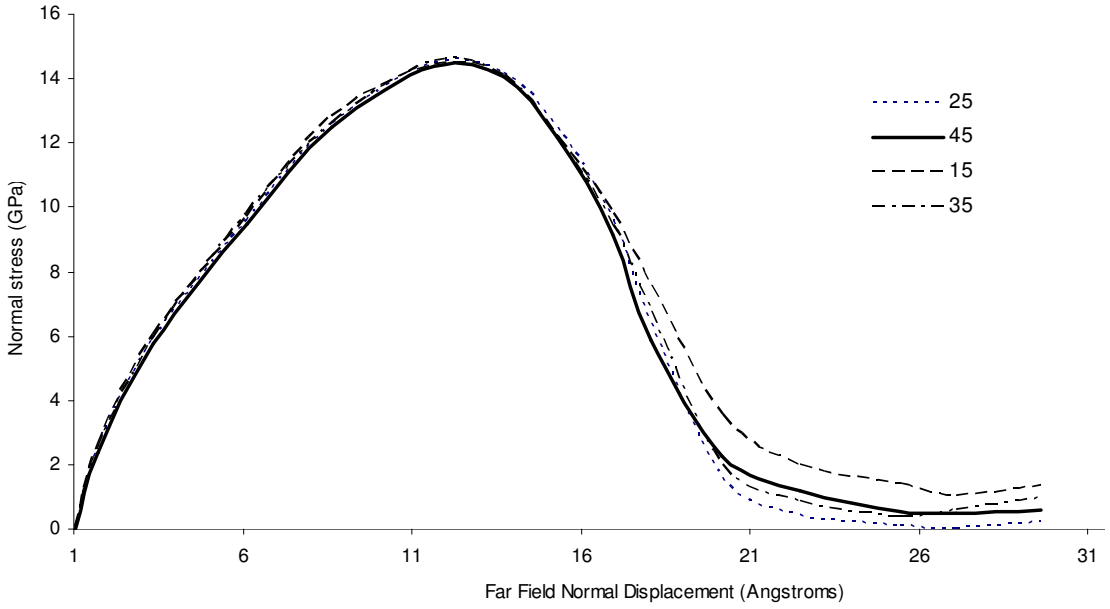

FIG. 4: Normal stress displacement response for various misorientation angles (in degrees) for the tilt GB

stress displacement response curves for a set of bicrystals with varying degrees of misorientations 15, 25, 35, and 45 deg loaded at a set temperature of 350 K. The displacement associated with peak stress is the same for all these cases. It is seen that peak stress reaches a minimum at a misorientation angle of 45 deg. Note that for a fcc bicrystal, a 45 deg misorientation represents the maximum tilt angle between the two crystals. The slope of the elastic part of the deformation is nearly uniform over the range of misorientations.

Figure 5 plots the tangential stress displacement response curves for 45 deg bicrystal loaded at a temperature of 300 K. Although the critical displacement for tensile mode and the shear mode occurs between 1 and 2 nm, the peak stresses for the shear mode are much smaller compared to the tensile mode. In addition, the softening part of the traction separation law occurs for a much longer duration and zero stresses are not reached until about 31.7 nm (compared to 2.125 nm for tensile loading case).

It is to be noted that shear simulations contain free boundaries along the yz planes. We note that the application of free boundaries may lead to a softer response (compared to that experienced by an equivalent cohesive element) owing to absorption of dislocations through rearrangement of atoms along the free surfaces. In addition, we note that the MD simulation is performed at the rate of 0.1 nm/ps whereas the continuum model is assumed to be rate independent. We performed molecular simulations at strain rates of 0.1 and 0.001 nm/ps to identify deformation rate effects. Over two orders of magnitude decrease in deformation rate, the decrease in peak stress was modest ($\sim 4.6\%$). The slope of the elastic part of the traction separation law was unchanged over these strain rates. The critical displacement (at peak stress) increased by 10.3% while fracture energy decreased by 11.6% over the two orders of magnitude decrease in deformation rate. Although a rate-dependent constitutive models based on grain boundary shearing rates [or based on Coble-type creep mechanisms (Yamakov et al., 2002)] are being developed (Wei et al., 2006), in this paper we restrict ourselves to a simpler rate-independent model. Indeed, the physical experiments at quasistatic strain rates (Torre et al., 2002) also reveal only a very slight strain rate sensitive response (in the case of nanocrystalline nickel). Such small strain rates can be accessed through molecular statics simulations (Warner et al., 2006) or through development of scaling laws [e.g., based on Zener-Holloman scaling (Zener et al., 1944)]. Nevertheless, continuum models cannot be directly verified without atomistic calculations because their validity is contingent on the accuracy of parameters used in the model.

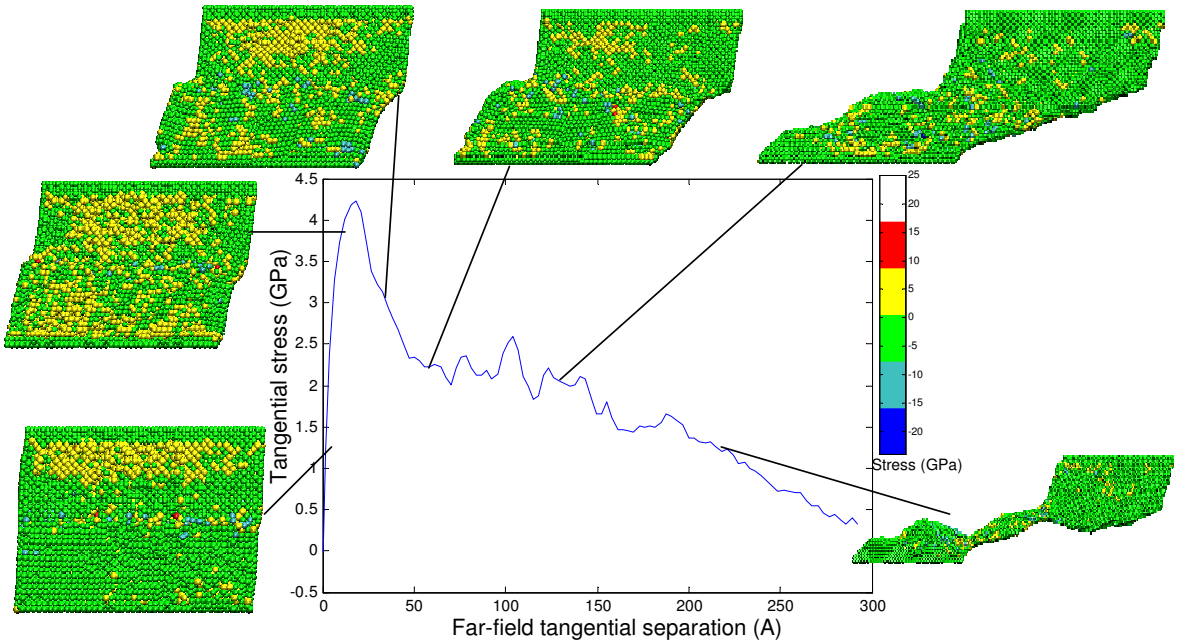

FIG. 5: Tangential stress versus displacement plot of the interface model in shear mode of separation.

3.2 Construction of Continuum Model Parameters

We consider nanocrystalline fcc copper with slip occuring in the 12 $\{111\}\langle 110\rangle$ slip systems. The anisotropic elasticity tensor for fcc copper can be specified in terms of the three stiffness parameters as $c_{11} = 170$ GPa, $c_{12} = 124$ GPa, and $c_{44} = 75$ GPa. Interface stiffnesses, K_N and K_T are defined based on the values of isotropic polycrystalline Young's modulus (E) and shear modulus (G) of copper and an assumed grain boundary thickness (g) of 1 nm as $K_N = E/g$ and $K_T = G/g$ which leads to values of $K_N = 130$ GPa/nm and $K_T = 48$ GPa/nm. The slip system resistance for grain interiors is calculated based on the notion that the grain boundaries are the sources of dislocations and the grain interiors are free of dislocations. The criterion for grain boundary emission and absorption of dislocations in nanocrystals is provided in (Wei et al., 2004) as $s^{\alpha} = G'b/D$, where $G' = \sqrt{(c_{11} - c_{12})c_{44}/2}$, b is the magnitude of Burgers vector, and D is the average grain size. This represents a criteria for grain boundary emission and absorption of dislocations in nanocrystalline polycrystals (Asaro et al., 2003). For fcc copper, these values are $G' = 41.5$ GPa and $b = 0.26$ nm. Additionally, initial elastic region (linear regime) in the cohesive law and was assumed to be valid up to a nominal stress of 1 GPa in both tensile and shear mode beyond which hardening begins (i.e., $s_0^{(1)} = s_0^{(2)} = 1$ GPa).

To effectively address the dependence of separation on interface structure, the set of state variables should incorporate parameters that describe physical attributes such as composition, dislocation density, and a measure of the number density of broken bonds (damage parameters) within the interfacial separation boundary layer. In the adopted model (Wei et al., 2004), a simplified practical description is provided using state variables that govern evolution of resistance of interface to deformation [Eq. (11)]. The parameters for inelastic response of the interface are obtained by systematically analyzing various regimes (initial elastic followed by hardening and softening) in a traction-separation curve predicted from molecular dynamics simulations. Key parameters of interest for the fitting procedure are the peak stress (t_N and t_T), critical displacement ($\delta_{c(N)}$ and $\delta_{c(T)}$) and the area under the cohesive law (fracture energy) for the interface under tension and shear modes at a misorientation of 45 deg and at a temperature of 300 K.

The following state variables at the interface are constructed from molecular calculations: The hardening exponent a^i, threshold resistance $s^{*(i)}$, hardening coefficient $h_0^{(i)}$, softening coefficient $h_{\text{soft}}^{(i)}$, effective displacement to failure $\bar{\gamma}_{\text{fail}}$, critical displacement $\bar{\gamma}_c$, and normal/tangential coupling parameter α.

A value of the coupling parameter $\alpha = 0.3932$ is obtained based on an assumed $\bar{\gamma}_c = 1.16$ nm, which is the critical displacement in tensile mode obtained from MD simulations. This value of the coupling parameter leads to a value of $\bar{\gamma}_c = 1.85$ nm when the interface starts to soften in shear (as observed from molecular simulations). The slope of the initial hardening region of the cohesive law (region up to the peak stress) was varied until it matched the molecular simulation result. The threshold resistance $[s^{*(i)}]$ was subsequently varied until the peak stress as predicted by MD simulation is achieved. A simple linear evolution law is assumed for the evolution of interfacial resistance $a^{(i)} = 1$. This reduces the optimization problem of determining the state variables to the determination of two parameters: $[\bar{\gamma}_{\text{fail}}, h_{\text{soft}}^{(1)}]$ subject to the constraints that the variables are positive and $\boldsymbol{t} = 0$ for $\bar{\gamma} > \bar{\gamma}_{\text{fail}}$. The objective was to minimize the error in the area under the cohesive law predicted by the cohesive model. The values obtained through this procedure are listed in Tables 1 and 2. The final traction separation response obtained is shown in Fig. 6.

In a related work (Spearot et al., 2004), the validity of the cohesive laws was tested during the unloading and reloading process in Cu nanobicrystal. The unloading behavior is a long-time behavior and needs to be analyzed using quasistatic or long-time molecular dynamics simulations. From results of MD simulations, it was postulated that although tangential separation produces a residual plastic displacement upon unloading, the normal mechanism would unload to zero displacement elastically while retaining the original interface strength. In the shear separation mode, the continuum cohesive model performs as expected. However, in the normal separation mode, the continuum law leads to a permanent plastic displacement

TABLE 1: For bicrystal Cu, the following continuum parameters were calibrated from MD simulations

Parameter	Value
Peak stress in tension (GPa)	14.50
Peak stress in shear (GPa)	4.23
Critical displacement in tension (nm)	1.16
Critical displacement in shear (nm)	1.85
Failure displacement in tension (nm)	2.125
Failure displacement in shear (nm)	31.7

TABLE 2: For bicrystal Cu, the following parameters were identified from MD simulations

Parameter	Value
Hardening exponent	$a^{(1)} = a^{(2)} = 1$
Threshold resistance	$s^{*(1)} = 20$ GPa and $s^{*(2)} = 4.7$ GPa
Hardening coefficient	$h_0^{(1)} = 21$ GPa/nm and $h_0^{(2)} = 8.3$ GPa/nm
Softening coefficient	$h_{\text{soft}}^{(1)} = 14$ GPa/nm and $h_{\text{soft}}^{(2)} = 0.3$ GPa/nm
Effective displacement to failure	$\bar{\gamma}_{\text{fail}} = 16.0$ nm
Critical displacement	$\bar{\gamma}_{\text{critical}} = 1.16$ nm
Normal/tangential coupling parameter	$\alpha = 0.3932$

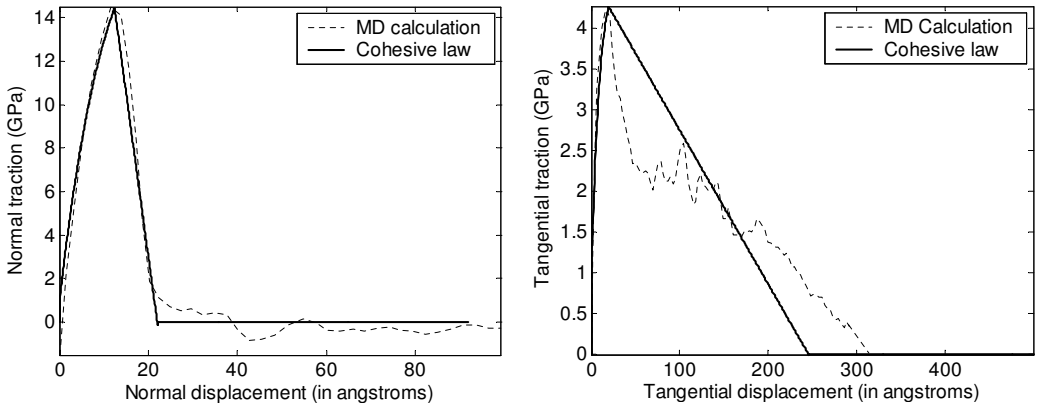

FIG. 6: Depiction of traction-displacement laws identified for simulation of grain boundary sliding and separation.

upon unloading. Upon reloading, the continuum cohesive law follows the original curve from the point at which it was unloaded.

The unloading and reloading behavior in the normal separation mode was tested using molecular simulations and the results are shown in Fig. 7. The zero force constraint and velocity boundary conditions on the top and bottom boundary planes were removed to simulate the unloading process. Upon release of the load, the normal stress relaxes almost immediately. This is followed by a dynamic behavior where the inward momentum of atoms at the outward boundaries competes with the outward momentum of atoms at the crack and the system elastically rebounds. Over a long time, these oscillations die down and the system slowly relaxes back such that the interface is regenerated. The configuration of atoms during the unloading and the associated per atom stresses are shown in Fig. 7. A small amount of residual plastic deformation is seen after the elastic oscillations die down (after 1 ns simulation time). Upon reloading, the system follows a cohesive law similar in nature to the original cohesive law, although with a relatively smaller peak stress. In a real system, dislocations that are emitted from the interface region have the ability to sweep further away from their source. It is noted that MD model is sensitive to the size of the domain used and the use of a restricted domain would mask the larger length scales involved in plasticity (dislocation motion). The use of fixed boundaries would, in fact, drive the dislocations emitted back to the crack, which can affect the relaxation behavior. Clearly, there is further scope for interpretation of molecular simulation results to understand unloading and reloading behavior in quasistatic regimes.

4. CONTINUUM RESPONSE PREDICTION

Standard crystal plasticity models for intragranular deformation is inadequate to represent limited plasticity [e.g., one or two dislocation partials] in nanocrystalline materials. However, elastic anisotropy and crystallographic texture are still important considerations since the dislocations are expected to move on the slip systems. Crystal-

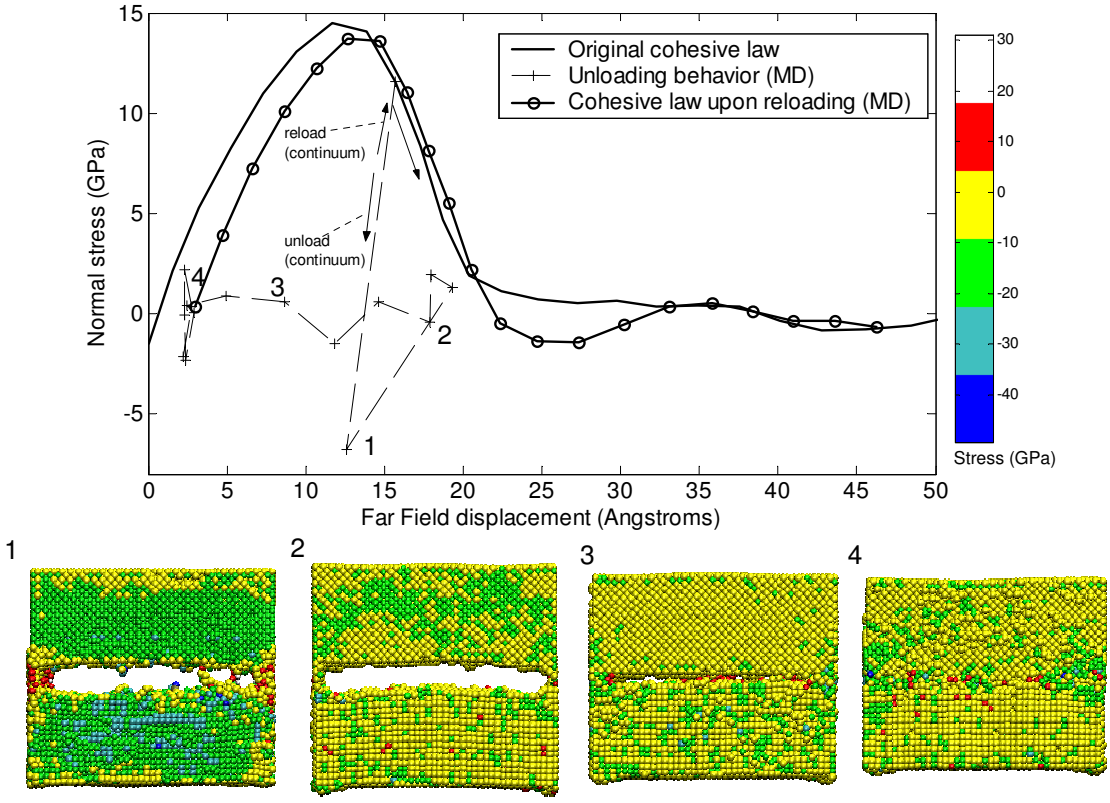

FIG. 7: Depiction of normal traction-displacement laws in the case of unloading. The figure identifies discrepancies in the model used in Wei and Anand (2004) and molecular dynamics model. The atom configuration at various points during unloading are indicated

lographic slip and reorientation of crystals are modeled in this work using a rate-independent constitutive model (Anand and Kothari, 1996). It is assumed that deformation takes place through dislocation glide and the evolution of the plastic flow is given by

$$\boldsymbol{L}^p = \dot{\boldsymbol{F}}^p(\boldsymbol{F}^p)^{-1} = \sum_{\alpha} \dot{\gamma}^{\alpha} \boldsymbol{S}_0^{\alpha} sign(\tau^{\alpha}) \qquad (16)$$

where $\boldsymbol{S}_0^{\alpha} = \boldsymbol{m}^{\alpha} \otimes \boldsymbol{n}^{\alpha}$ is the Schmid tensor and $\dot{\gamma}^{\alpha}$ is the plastic shearing rate on the α^{th} slip system. $\boldsymbol{m}^{\alpha}$ and $\boldsymbol{n}^{\alpha}$ are the slip direction and the slip plane normal, respectively. In the constitutive equations to be defined next, the Green elastic strain measure (defined on the plastically deformed stress-free configuration) is utilized,

$$\tilde{\boldsymbol{E}}^e = \frac{1}{2}\left(\boldsymbol{F}^{eT}\boldsymbol{F}^e - \boldsymbol{I}\right) \qquad (17)$$

A conjugate stress measure is then defined as

$$\tilde{\boldsymbol{T}} = \det\boldsymbol{F}^e(\boldsymbol{F}^e)^{-1}\boldsymbol{T}(\boldsymbol{F}^e)^{-T} \qquad (18)$$

where $\boldsymbol{T}$ is the Cauchy stress for the crystal in the sample reference frame. The constitutive relation for the stress measure is given by

$$\tilde{\boldsymbol{T}} = \boldsymbol{\mathcal{L}}^e\left[\tilde{\boldsymbol{E}}^e\right] \qquad (19)$$

where $\boldsymbol{\mathcal{L}}^e$ is the fourth-order anisotropic elasticity tensor for fcc Cu (Anand and Kothari, 1996), expressed in terms of the crystal stiffness parameters and the orientation $\boldsymbol{r}$. The resolved shear stress $\boldsymbol{\tau}^{\alpha} = \tilde{\boldsymbol{T}} \cdot \boldsymbol{S}_0^{\alpha}$ attains a critical value s^{α} on the systems where slip occurs with plastic shearing rate on the α^{th} slip system $\dot{\gamma}^{\alpha} > 0$. Furthermore, the resolved shear stress does not exceed s^{α} on the inactive systems with $\dot{\gamma}^{\alpha} = 0$. Thus, the following relation holds:

$$|\boldsymbol{\tau}^{\alpha}| - s^{(\alpha)} = 0 \;\text{ for }\; \dot{\gamma}^{\alpha} > 0 \tag{20}$$

Slip system resistances (Wei and Anand, 2004) are assumed to be constants, i.e., $\dot{s}^{\alpha}(i) = 0$.

A polycrystal (Fig. 8) with 64 grains was generated using a standard Voronoi construction employed in the design examples of Sundararaghavan and Zabaras (2006b). Based on $s^{\alpha} = G'b/D$ as explained previously, and average grain size of $D = 26$ nm leads to a slip system resistance of 415 MPa. To overcome the dependency of the solution on the mesh size, the polycrystal was meshed at the highest mesh density using our inhouse meshing tool, which led to 19,525 quadrilateral elements, including the four-noded zero-thickness cohesive zone elements at the grain boundaries. Random orientations were assigned to the grains such that all grain boundaries were of tilt character. The polycrystal was subjected to tensile loading along the y direction. In this work, the equivalent strain is computed based on the volume average of the deformation rate ($\bar{\boldsymbol{D}} = \langle \boldsymbol{D} \rangle$). The average effective plastic strain $\bar{\epsilon}_{\text{eff}}$ is defined as $\bar{\epsilon}_{\text{eff}} = \int_0^t \sqrt{2/3 \bar{\boldsymbol{D}} \cdot \bar{\boldsymbol{D}}} dt$. The equivalent stress for the polycrystal is represented using the von Mises norm $\bar{\sigma} = \sqrt{(3/2)\tilde{\boldsymbol{T}}' \cdot \tilde{\boldsymbol{T}}'}$, $\tilde{\boldsymbol{T}}' = \tilde{\boldsymbol{T}} - 1/3 tr(\tilde{\boldsymbol{T}})\boldsymbol{I}$.

Figure 9 provides the stress contour and the equivalent stress strain curve when plastic strains are first observed. As the separation progresses, high stresses develop close to sharp crack corners, as seen in Fig. 9(a). The crack path followed during this uniaxial loading process occurs approximately at the midline of the polycrystal. In Fig. 9(b), we also show the equivalent stress strain curve when grain boundary deformation modes are deactivated (cohesive elements are removed). The plastic yielding begins at a much larger stress when grain boundary accommodation effects are not accounted for. The equivalent plastic strain plots in Fig. 10 clearly indicate the role of interfaces in nanocrystals. The initial plastic response observed at the nanoscale was localized at regions of grain boundary cracks, especially at the sharp crack tips. As seen from Fig. 10, the interior of grains show no sign of plastic strains while crack tips are the zone for plastic deformation. This result is agreeable with results (Wei and Anand, 2004) that reveal that the macroscopically imposed deformation is initially accommodated by grain boundary accommodation effects. Note that the initial yield strength of 26 nm Cu polycrystal is observed at 340 MPa (compared to 365 MPa value experimentally identified in several other papers (Sanders et al., 1997; Gertsman et al., 1994; Suryanararayan et al., 1996). The grain boundary sliding and separation effects at such locations of high plastic strains are shown in Fig. 10. This reveals that when grain boundary deformation cannot be accommodated due to geometric restrictions at locations of crack tips or triple junction in Fig. 10, local stress concentrations develop to cause plastic strains (dislocation emission) at these locations. Please note that a crystal plasticity-based description of the inelastic deformation of the grain interior for nanocrystalline materials does not account for the emission or absorption of dislocations from grain boundaries. The simulations do not show significant plastic strain in the interior of grain, and the interior of the grains can be considered elastic during the initial part of the stress strain curve. In light of some of discrepancies mentioned previously in the continuum model and the molecular simulation results (notably, unloading behavior, finite size, strain rate effects, and intragranular plasticity laws), further study is still necessary before comparing stress-strain curves based on calibrated continuum laws with experiments performed at quasistatic strain rates.

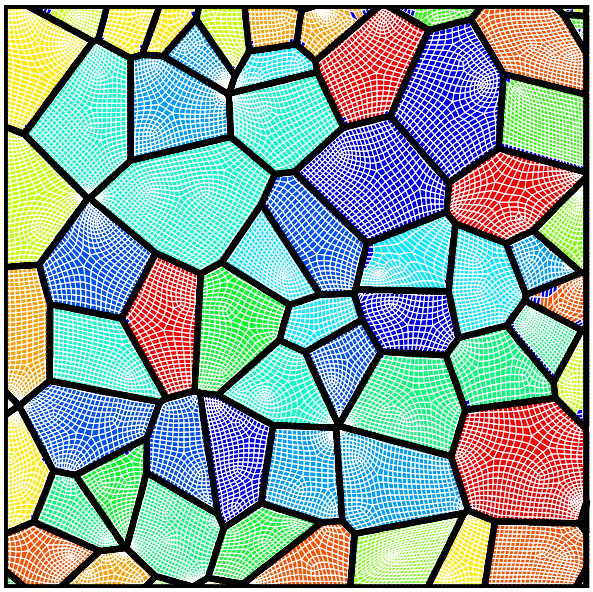

FIG. 8: Initial polycrystal for the crack problem with 64 grains. Initial texture was randomly assigned.

5. CONCLUSIONS

This paper presents an initial study of the use of MD simulations to calibrate an isothermal, rate-independent elasticplastic grain boundary model for pure nanocrystalline copper. The continuum model introduces a variety

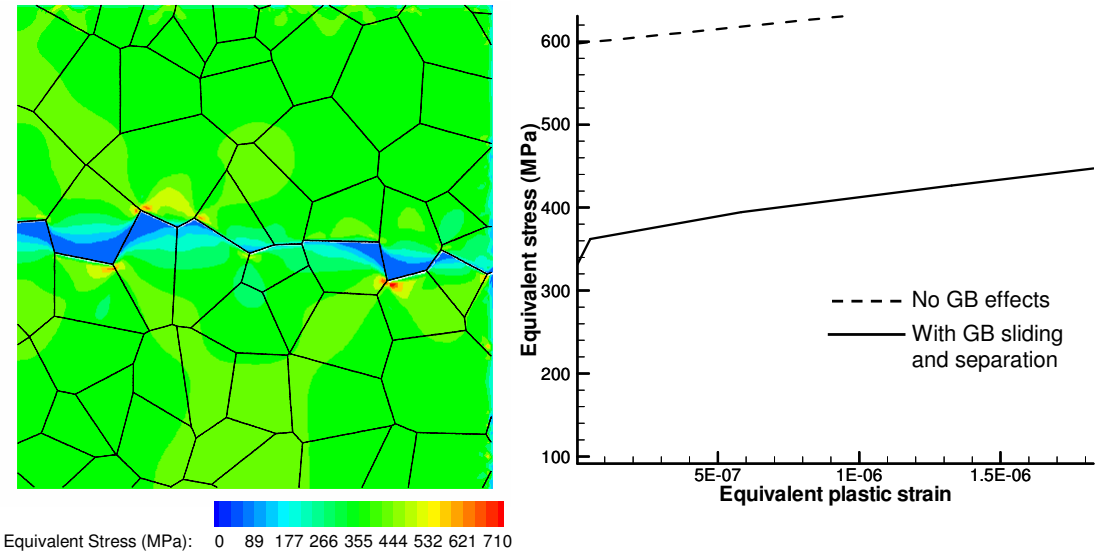

FIG. 9: The stress contours for the polycrystal. The initial plastic strain is due to the effect of grain boundaries. The curve obtained when grain boundaries are deactivated is also shown.

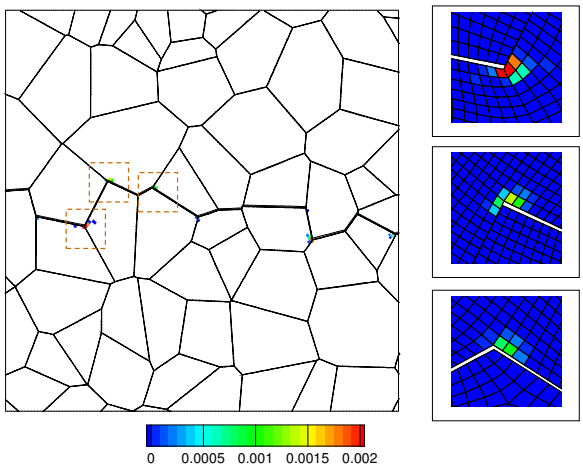

FIG. 10: The plastic strain locations during initiation of plasticity. The plastic strains are concentrated on grain boundary triple points or sharp corners

of new physics compared to existing models, including irreversible plastic deformation prior to failure and ability to explain combined shear and tensile loading behavior. To guide the continuum formulation, atomistic calculations are presented for a planar, copper grain boundary interface with a tilt lattice misorientation. The interface models are deformed to full separation with both tensile and shear deformations. Plots of stress versus displacement show a distinctly different deformation response between normal and tangential interface loading conditions. It is seen that loading that promotes tensile separation exhibits a rapid increase in stresses, while shear deformation of the interface region produces a much slower evolution rate and smaller stresses by comparison. Furthermore, MD simulations provide us with traction separation laws that account for dependence on grain boundary misorientations and deformation rates.

The data were used to calibrate the state variables in the traction separation law. Microstructures simulated using cohesive model of the grain boundary indicates that the macroscopically observed nonlinearity in the stress-strain response is mainly due to the inelastic response of the grain boundaries. Plastic deformation in the interior of the grains prior to the initiation of grain boundary cracks was not observed. The stress concentrations at the tips of the distributed grain boundary cracks, and at grain boundary triple junctions, cause a limited amount of plastic deformation in the high-strength grain interiors. However, some discrepancies were noted when the results of unloading and reloading in the continuum model are compared to molecular simulations. The continuum model models irreversible inelastic normal separation at the interface prior to failure. Results from long-time MD sim-

ulations indicate that cracks formed due to normal loads would unload to zero displacement elastically while retaining the original interface strength. Clearly, there is merit for future study in examining traction separation behavior under long-time relaxation and reloading processes. However, the size of the domain and the strain-rate effects need to be carefully accounted for to accurately model the phenomena at continuum scales.

ACKNOWLEDGEMENTS

This work was sponsored by NASA Constellation University Institutes Project under Grant No. NCC3-989 with Claudia Meyer as the project manager.

REFERENCES

Anand, L. and Kothari, M., A computational procedure for rate-independent crystal plasticity, *J. Mech. Phys. Solids*, vol. **44**, pp. 525–558, 1996.

Asaro, R. J., Krysl, P., and Kad, B., Deformation mechanism transitions in nanoscale fcc metals, *Philos. Mag. Lett.*, vol. **83**, pp. 733-743, 2003.

Camacho, G. T. and Ortiz, M., Adaptive Lagrangian modelling of ballistic penetration of metallic targets, *Comput. Methods Appl. Mech. Eng.*, vol. **142**, pp. 269-301, 1997.

Cleri, F., Yip, S., Wolf, D., and Phillpot, S. R., Atomic-scale mechanism of crack-tip plasticity: Dislocation nucleation and crack-tip shielding, *Phys. Rev. Lett.*, vol. **79**, pp. 1309-1312, 1997.

Cleri, F., Phillpot, S. R., Wolf, D., and Yip, S., Atomistic simulations of materials fracture and the link between atomic and continuum length scales, *J. Amer. Ceramic Soc.*, vol. **81**(3), pp. 501–516, 1998.

Daw, M. S., Foiles, S. M., and Baskes, M. I., The embedded atom method: A review of theory and applications, *Mater. Sci. Rep.*, vol. **9**(7–8), p. 251–310, 1993.

Fu, H.-H., Benson, D. J., and Meyers, M. A., Computational description of nanocrystalline deformation based on crystal plasticity, *Acta Mater.*, vol. **52**, pp. 4413–4425, 2004.

Gall, K., Iesulauro, E., Hui, H., and Ingraffea, A., Atomistic and continuum based fracture modeling in single crystal silicon, *Tech. Science Press.*, Encino, CA, 2000.

Gertsman, V. Y., Birringer, R., Valiev, R. Z., and Gleiter, H., On the structure and strength of ultrafine grained copper produced by severe plastic deformation, *Scripta Metall. Mater.*, vol. **30**, pp. 229–235, 1994.

Holian, B. L. and Ravelo, R., Fracture simulations using large-scale molecular dynamics, *Phys. Rev. B*, vol. **51**, pp. 11275–11288, 1995.

Horstemeyer, M. F., Baskes, M. I., and Plimpton, S. J., Length scale and time scale effects on the plastic flow of FCC metals, *Acta Mater.*, vol. **49**, pp. 4363-4374, 2001.

Kumar, K. S., Suresh, S., Chisolm, M. F., Horton, J. A., and Wang, P., Deformation of electodeposited nanocrystalline nickel, *Acta Mater.*, vol. **51**, pp. 387-405, 2003.

Nakano, A., Kalia, R. K., and Vashishta, P., Growth of pore interfaces and roughness of fracture surfaces in porous silica: Million particle molecular-dynamics simulations, *Phys. Rev. Lett.*, vol. **73**, pp. 2336–2339, 1994.

Needleman, A., An analysis of tensile decohesion along an interface, *J. Mech. Phys. Solids*, vol. **38**, pp. 289-324, 1990.

Needleman, A., Micromechanical modeling of interfacial decohesion, *Ultramicroscopy*, vol. **40**, pp. 203-214, 1992.

Ortiz, M. and Pandolfi, A., A class of cohesive elements for the simulation of three-dimensional crack propagation, *Int. J. Numer. Methods Eng.*, vol. **44**, pp. 1267-1282, 1999.

Plimpton, S. J., Fast parallel algorithms for short-range molecular dynamics, *J. Comp. Phys.*, vol. **117**, pp. 1–19, 1995.

Rice, J. R., Dislocation nucleation from a crack tip: An analysis based on the peierls concept, *J. Mech. Phys. Solids*, vol. **40**, pp. 239-271, 1992.

Sanders, P. G., Eastman, J. A., and Weertman, J. R., Elastic and tensile behavior of nanocrystalline copper and palladium, *Acta Mater.*, vol. **45**(10), pp. 4019–4025, 1997.

Schiotz, J., Vegge, T., Tolla, F. D. D., and Jacobsen, K. W., Atomic-scale simulations for the mechanical deformation of nanocrystalline metals, *Phys. Rev. B*, vol. **60**, pp. 11197-11983, 1999.

Spearot, D. E., Jacob, K. I., and McDowell, D. L., Non-local separation constitutive laws for interfaces and their relation to nanoscale simulations, *Mech. Mater.*, vol. **36**(9), pp. 825–847, 2004.

Sundararaghavan, V. and Zabaras, N., Combined MD and continuum approaches towards modeling inter-granular failure using cohesive zone models, Deformation and Fracture from Nano to Macro: A Symposium Honoring W.W. Gerberich's 70th Birthday, TMS Annual Meeting and Exhibition, San Antonio, 2006a.

Sundararaghavan, V. and Zabaras, N., Design of microstructure-sensitive properties in elasto-viscoplastic polycrystals using multi-scale homogenization, *Int. J. Plasticity*, vol. **22**, pp. 1799–1824, 2006b.

Suryanarayanan, R., Frey, C. A., Sastry, S. M. L., Waller, B. E., Bates, S. E., and Buhro, W. E., Mechanical properties of nanocrystalline copper produced by solution-phase synthesis, *J. Mater. Res.*, vol. **11**, pp. 439–448, 1996.

Swygenhoven, H. V., Spaczer, M., Caro, A., and Farkas, D., Competing plastic deformation mechanisms in nanophase metals, *Phys. Rev. B*, vol. **60**, pp. 22-25, 1999.

Swygenhoven, H. V., Plastic deformation in metals with nano-

sized grains: Atomistic simulations and experiments, *Mater. Sci. Forum*, vol. **447–448**, pp. 3-10, 2004.

Torre, F. D., Swygenhoven, H. V., and Victoria, M., Nanocrystalline electrodeposited Ni: Microstructure and tensile properties, *Acta Mater.*, vol. **50**, pp. 3957-3970, 2002.

Tvergaard, V. and Hutchinson, J. W., The influence of plasticity on mixed-mode interface toughness, *J. Mech. Phys. Solids*, vol. **41**, pp. 1119-1135, 1993.

Tvergaard, V. and Hutchinson, J. W., Effect of strain dependent cohesive zone model on predictions of crack growth resistance, *Int. J. Solids Struct.*, vol. **33**, pp. 3297-3308, 1996.

Warner, D. H., Sansoz, F., and Molinari, J. F., Atomistic based continuum investigation of plastic deformation in nanocrystalline copper, *Int. J. Plasticity*, vol. **22**(4), pp. 754–774, 2006.

Wei, Y. J. and Anand, L., Grain-boundary sliding and separation in polycrystalline metals: Application to nanocrystalline fcc metals, *J. Mech. Phys. Solids*, vol. **52**(11), pp. 2587–2616, 2004.

Wei, Y., Su, C., and Anand, L., A computational study of the mechanical behavior of nanocrystalline fcc metals, *Acta Mater.*, vol. **54**, pp. 3177–3190, 2006.

Willam, K., Simulation issues of distributed and localized failure computations, *Cracking and Damage*, Mazars, J. and Bazant, Z. P., Eds, Elsevier, New York, pp. 363-378, 1989.

Xu, X. P. and Needleman, A., Numerical simulations of fast crack growth in brittle solids, *J. Mech. Phys. Solids*, vol. **42**, pp. 1397-1434, 1994.

Yamakov, V., Saether, E., Phillips, D. R., and Glaessgen, E. H., Molecular-dynamics simulation-based cohesive zone representation of intergranular fracture processes in aluminum, *J. Mech. Phys. Solids*, vol. **54**(9), pp. 1899–1928, 2006.

Yamakov, V., Wolf, D., Salazar, M., Phillpot, S. R., and Gleiter, H., Length-scale effects in the nucleation of extended dislocations in nanocrystalline Al by molecular-dynamics simulation, *Acta Mater.*, vol. **49**, pp. 2713-2722, 2001.

Yamakov, V., Wolf, D., Phillpot, S. R., and Gleiter, H., Grain-boundary diffusion creep in nanocrystalline palladium by molecular-dynamics simulations, *Acta Mater.*, vol. **50**, pp. 61-73, 2002.

Zavattieri, P. D. and Espinosa, H. D., Grain level analysis of crack initiation and propagation in brittle materials, *Acta Mater.*, vol. **49**, pp. 4291–4311, 2001.

Zener, C. and Hollomon, J. H., Effect of strain rate upon plastic flow of steel, *J. Appl. Phys.*, vol. **15**, pp. 22–26, 1944.

Zhou, S. J., Lomdahl, P. S., Voter, A. F., and Holian, B. L., Three-dimensional fracture via large-scale molecular dynamics, *Eng. Fract. Mech.*, vol. **61**, pp. 173–187, 1998.